β-Cyclodextrin-bearing Gold Glyconanoparticles for the Development of Site Specific Drug Delivery Systems

*Ahmet Aykaç, Manuel C. Martos-Maldonado, Juan M. Casas-Solvas, Indalecio Quesada-Soriano, Federico García-Maroto, Luís García-Fuentes, and Antonio Vargas-Berenguel**

Department of Chemistry and Physics, University of Almería, Carretera de Sacramento s/n, 04120 Almería, Spain.

*Corresponding author. E-mail: avargas@ual.es. Phone: (+34) 950 015619. Fax: (+34) 950 015008.

ABSTRACT. Three novel gold nanoparticles containing multiple long, flexible linkers decorated with lactose, β-cyclodextrin and both simultaneously have been prepared. The interaction of such nanoparticles with β-D-galactose-recognizing lectins peanut agglutinin (PNA) and human galectin-3 (Gal-3) was demonstrated by UV-Vis studies. Gal-3 is well-known to be overexpressed in several human tumors and can act as biorecognizable target. This technique also allowed us to estimate their loading capability toward the anticancer drug methotrexate (MTX). Both results make these glyconanoparticles potential site-specific delivery systems for anticancer drugs.

INTRODUCTION

In the last 15 years gold nanoparticles (AuNPs)[1] have found increasing application as biomarkers for diagnose and imaging, drug delivery systems and sensors for detection of proteins, metal ions, DNA, carbohydrates, viruses and different classes of cells. This is due to their ability to act as scaffolds for different biomolecules using thiol surface self-assembly monolayers (SAMs) chemistry.[2-6] AuNPs present a high flexibility in terms of linker nature (rigidity and polarity) and ligand density of distribution on the surface. In addition, they can be multifunctionalised with more than one sort of appendages on the same particle very easily. The size of the AuNPs between 1 and 100 nm is in the range of those biomacromolecules so they can serve as biomimetic and biofunctional materials inside cells. In addition, optical, electronic and magnetic properties of AuNPs allow them to highlight supramolecular and recognition processes. Probably the best well-known property is the Surface Plasmon Resonance (SPR) phenomenon which can be observed in the visible region as a broad absorption band around 520 nm giving their water solutions a deep-red colour. This band does not exist for AuNPs smaller than 2 nm and quickly shifts to longer wavelengths for AuNPs larger than 20 nm. It is also sensitive to the nature of the substituent self-assembled on their surface, the dielectric constant of the environment and the inter-particle distance.

As drug nanocarriers, AuNPs enable the protection of the drug against degradation or inactivation in biological conditions and in some cases the design of controlled release methods upon the application of external stimuli.[7] Drugs can be covalently attached on the AuNP surface, but this requires the chemical modification of the drug for the anchoring and, quite often, some intracellular processing or external stimuli (heat, light) of the resulting conjugate for the drug release. In contrast, unmodified drugs can be non-covalently loaded onto the AuNP by

appending on its surface amphiphilic linkers able to create hydrophobic pockets within the monolayer,[7] or suitable macrocyclic molecular receptors such as cyclodextrins.[8-11] β-Cyclodextrin (β-CD) is a natural occurring, torus-shaped, cyclic oligosaccharide comprising seven D-glucopyranose units linked by α-(1→4) bonds. β-CD and its derivatives are well-known to form inclusion complexes in aqueous solution with a large variety of organic molecules of hydrophobic nature and suitable size and geometry encompassing several anti-cancer drugs.[12-16] In addition, the presence of β-CD on the AuNP may also help to overcome certain forms of multidrug resistance.[17-19]

AuNPs surface can be modified with different biomolecules which specifically interact with receptors that are over-expressed in cancer cells in order to selectively cumulate on them. This strategy not only allows increasing the delivery of the drug to tumor cells but also enables new therapy techniques such as optical microscopy, multi-absorption-induced-luminescence (MAIL), photothermal therapy (PTT) and radiotherapy.[20,21] In particular, carbohydrate-coated gold nanoparticles (glycoAuNPs) have been successfully used for studying carbohydrate-protein binding processes.[3] Attaching carbohydrates on the AuNPs not only improve their biocompatibility and water solubility but also increase their targeting ability. It is well-known that several proteins called lectins, which act as carbohydrate specific receptors, are overexpressed on the cancer cells surface. A particularly interesting lectin is human galectin-3 (Gal-3), which recognizes and binds β-D-galactoseide moieties, and plays a role in tumor progression and metastasis enhancing survival upon exposure to different apoptotic stimuli. Thus, Gal-3 could be used as a site-specific target for β-D-galactose- or lactose-appended glycoAuNPs.[22]

In this context, we envisaged a dually functionalized AuNP bearing simultaneously multiple copies of β-D-lactose units as targeting ligands for Gal-3, and β-CD macrocycles as encapsulating moieties for suitable anticancer drugs (Scheme 1). Site-specific drug carriers based on cyclodextrins-coated AuNPs have been recently described using anti-epidermal growth factor receptor antibody (anti-EGFR)[9,10] and biotin[11] as vectors. Although concurrent presentation of carbohydrates and β-CD is well-known on glyconjugates, glycodendrimers, glycopolymers, micelles and vesicles for the construction of water soluble site-specific delivery systems,[23,24] to the best of our knowledge such combination on gold nanoparticles has not been previously described. AuNPs allow for a multivalent presentation of the carbohydrates, a well-known strategy used to overcome the low binding affinity between saccharides and proteins, enabling their use as site-specific delivery vectors. Multivalent presentation of cyclodextrin units would make possible the loading of anticancer drugs by both forming stable inclusion complexes and entrapping the drug between branches. Conveniently, carbohydrates do not compete with cyclodextrin guests for the CD cavity. We decided to include flexible, relatively long spacers between both appendages and the surface of the AuNP as a way to overcome steric hindrance and maximize the number of active carbohydrates and CD moieties.[25-27] We chose an hybrid tether consisting of an apolar thioundecylene chain anchored to the AuNP surface followed by a hydrophilic tetra(ethylene glycol) skeleton decorated with the appendages at its end. The lipophilic part provides stability to the SAM and may create additional entrapping sites for the drug, while the tetraglycol increases the biocompatibility and the solubility in water.[28] Such sort of mixed chains has recently showed enhanced ability of AuNPs for preventing non-specific protein adsorption, proteolytic and hydrolytic degradation, and macrophage uptaking.[29-31]

Thus, in this work we report the preparation of a gold nanoparticle **1**-**3** containing multiple copies of lactose, β-CD or both simultaneously (Scheme 1). The potential ability of such nanoparticles as targeted drug delivery systems was evaluated by studying their affinities for the β-D-galactose-recognizing lectins Gal-3 and PNA as biological targets by UV-Vis spectroscopy. Protein-induced aggregation of AuNPs is usually proven by a SPR band red-shift upon lectin addition in UV-Vis,[27,32-42] although other techniques have been used to gain deeper insight into this interaction and, in some cases, quantify the binding affinity as compared to simple glycosides.[43-47] The loading capability of nanoparticles **2** and **3** toward the anticancer drug methotrexate (MTX, Chart 1) was also estimated.

EXPERIMENTAL PROCEDURES

Materials. Thin layer chromatography (TLC) was performed on Merck silica gel 60 F254 aluminium sheets and developed by UV-Vis light and ethanolic sulfuric acid (5 % v/v). Flash column chromatography was performed on Merck silica gel (230-400 mesh, ASTM). Melting points were measured on a Büchi B-450 melting point apparatus and are uncorrected. Optical rotations were recorded on a Jasco P-1030 polarimeter at room temperature. $[\alpha]_D$ values are given in 10^{-1} deg cm^{-1} g^{-1}. Infrared spectra were recorded on a Bruker Alpha FTIR equipped with a Bruker universal ATR sampling accessory. ^{1}H and ^{13}C NMR spectra were recorded on Bruker Avance DPX300 and Bruker Avance 500 Ultrashield spectrometers equipped with a QNP $^{1}H/^{13}C/^{19}F/^{31}P$ and inverse TBI $^{1}H/^{31}P$/BB probe, respectively. Standard Bruker software was used for acquisition and processing routines. Chemical shifts are given in ppm and referenced to internal TMS (δ_H, δ_C 0.00). *J* values are given in Hz. MALDI-TOF mass spectra were recorded on a 4800 *Plus* AB SCIEX spectrometer with 2,5-dihydroxybenzoic acid (DHB) as the matrix. ESI-TOF mass spectra were measured on a Waters Xevo Qtof spectrometer. All aqueous

procedures used pure water (MilliQ, 18.2MΩ cm) obtained from a Millipore MilliQ Plus system. Dialysis was performed in MilliQ water using 3.500 kDa molecular weight cut-off (MWCO) membranes (Spectra/Por, regenerated cellulose). Centrifugal filtrations were carried out on a Digicen 21R centrifuge using Amicon Millipore 10.000 KDa MWCO and 3.000 KDa MWCO centrifugal filters for purification and concentration purposes, respectively. Dynamic Light Scattering (DLS) measurements were performed on a Zetasizer Nano ZS (Malvern Instruments Ltd, UK) with an Avalanche photodiode (QE > 50% at 633nm) detector, 173º scattering angle, class 1 compliant laser, and automatic laser attenuation. 15 nM AuNPs MilliQ water solutions were introduced in a 12μL quartz thermostated sample cuvette (low volume quartz ZEN2112) and experiments were carried out at 25 ºC by measuring 15 runs. Average hydrodynamic radius for each sample was calculated using standard Malvern Instruments software. Transmission Electron Microscopy (TEM) analyses were carried out on a Carl Zeiss LIBRA 120 PLUS instrument at 120 keV. Briefly, 20 μL of gold nanoparticle aqueous solution (*ca.* 0.1 mg mL^{-1}) were placed onto a copper grid coated with a carbon film. The grid was tapped with filter paper and dried in vacuum for 1 min. Negative staining was performed by using a droplet of 2% w/v uranyl acetate solution. Images were treated using Image Tool 3.0 software and at least 100 nanoparticles were measured to estimate the average diameter. All the glassware used for AuNPs was exhaustively washed with aqua regia, rinsed with MilliQ water and oven dried prior to use. All reagents, as well as peanut agglutinin from *Arachis hypogaea* (PNA, lyophilized powder, affinity-purified) and albumin from bovine serum (BSA, low endotoxin, lyophilized powder) lectins, were purchased from Sigma Aldrich and used without further purification. Compounds **4**,[32] **5**,[48] **6**[49] and $(EtO)_3P{\cdot}CuI$[49] were synthesised as previously reported. Solvents were dried according to literature procedures.[50]

Synthesis of citrate-stabilized AuNP. Citrate-stabilized AuNP (cAuNP) were prepared according to a modification[51] of the Turkevich protocol.[52] Briefly, a degassed solution of sodium citrate (228 mg, 0.775 mmol) in MilliQ water (20 mL) at 55 ºC was added to a refluxing degassed solution of $HAuCl_4 \cdot 3H_2O$ (79 mg, 0.201 mmol) in MilliQ water (200 mL) under vigorous stirring. The mixture was refluxed for 30 min and cooled to room temperature before being filtered through a Sartorius Minisart 0.2 μm filter to provided cAuNP of 12.1 ± 1.0 nm of average diameter in a concentration of ~13 nM, as determined by UV-Vis spectroscopy[53] and TEM.

General method for the synthesis of AuNPs 1-3. A solution of **9** (8 mg, 0.005 mmol) in MilliQ water (1 mL) for AuNP **1**, or a solution of **10** (16 mg, 0.005 mmol) in MilliQ water (1 mL) for AuNP **2**, or a mixture of **9** (8 mg, 0.005 mmol) and **10** (8 mg, 0.005 mmol) in MilliQ water (2 mL) for AuNP **3** were added to a ~13 nM solution of cAuNP in MilliQ water (5 mL). The resulting mixtures were stirred at room temperature for 16 hours in darkness. AuNPs **1-3** were purified by repetitive centrifugal filtrations through regenerated cellulose 10 MWCO filters at 3500 rpm for 30 min using MilliQ water as washing solution. UV-Vis spectra of each filtrate were recorded and filtration was repeated until negligible linker signal at λ 256 nm was observed in the last filtrate (5 times). Average diameter and concentration for each AuNP were determined by TEM and UV-Vis spectroscopy,[53] respectively.

Expression and purification of Gal-3. The cDNA clone for the human galectin-3 (Gal-3) was obtained from the ATCC collection (Cat. No. MGC-2058). For protein expression the coding sequence was amplified by PCR from the pOTB7 plasmid, using a high fidelity DNA polymerase (iProof, BioRad) and the oligonucleotides 5′-ACGCGGATCCATGGCAGACAATTTTTCGCTCCATGATGC-3′ and 5′-

ACCGGAATTCTTATATCATGGTATATGAAGCACTGGTGAGG-3′ containing appropriate restriction sites. The PCR fragment was cloned into the *Bam*HI and *Eco*RI sites of the pGEX-6P-1 expression vector (GE Healthcare Life Sciences) to generate a protein fusion with the glutathione S-transferase (GST). The recombinant plasmid was checked by sequencing and used to transform *E. coli* BL21 (DE-3) cells. GST-galectin-3 fusion protein was overexpressed in *E. coli* and purified by affinity chromatography on lactosyl-sepharose as previously described.[54] Lactose-derivatised Sepharose 6B was prepared by the divinylsulphone method of Porath and Ersson.[55] Cells were resuspended in PBS buffer containing a cocktail of proteases inhibitors (0.24 IU/mL aprotinin, 1 μg/mL leupeptin, 1 μg/mL benzamidine, 0.1 mg/mL lysozyme, 0.2 mM PMSF at 4 ºC. After sonication and centrifugation, the supernatant was loaded onto an equilibrated lactosyl-sepharose column in PBS buffer at 0.5 mL/min. The fusion protein was eluted with 10% (p/v) lactose in PBS buffer. Fractions with protein were joined, concentrated and dialysed twice against in cleavage buffer (50 mM Tris-HCl, 150 mM NaCl, 1 mM EDTA, 1 mM dithiothreitol at pH 7) and 4ºC. After dialysis, the protein sample was incubated overnight in the presence of 1% (v/v) *Prescission protease* (GE Healthcare Life Sciences) at 4 ºC. After digestion, the sample was applied again to washed and equilibrated lactosyl-sepharose column in cleavage buffer. Purified Gal-3 was obtained by elution with 10% (p/v) lactose in PBS and 1 mM DTT. Purification of Gal-3 was confirmed by SDS-PAGE. Protein concentration was determined by Bradford assay.[56] A molecular mass of 26 kDa was used for the monomeric Gal-3 enzyme.

UV-Vis spectroscopy measurements. UV-Vis spectra were recorded on a Jasco V-530 spectrophotometer at room temperature using 1 cm path-length 1 mL disposable plastic cuvettes. MilliQ water or 10 mM phosphate buffer at pH 7.2 containing 20 mM NaCl were used as

references depending on the case. Characterisation of cAuNP and AuNPs **1-3** was performed in MilliQ water solutions as described elsewhere.[53]

The interaction of AuNPs **1** and **3** with PNA and Gal-3 was measured on solutions of each nanoparticle (2 nM) in the presence of each protein (2 μM for the lectin monomer in the case of PNA and 50 μM for Gal-3) in 10 mM phosphate buffer solutions at pH 7.2 containing 20 mM NaCl. The UV-Vis spectra of the mixtures were recorded every 5 minutes after the addition of the lectin. After 5 hours, solid lactose was added to a final concentration of 40 mM and the solution was gently shaken. The UV-Vis spectra were then measured after 10 minutes. A solution of each nanoparticle (2 nM) in the absence of the lectin was also recorded as reference.

For the determination of the MTX loading abilities of AuNPs **2** and **3**, solutions of each nanoparticle (2 nM) and MTX (75 μM) were prepared in 10 mM phosphate buffer at pH 7.2 containing 20 mM NaCl (2 mL) and shaken at room temperature in darkness for 5 days. UV-Vis spectrum of each sample was measured and the excess of MTX was then removed by repetitive centrifugal filtration through regenerated cellulose 10 MWCO filters at 3500 rpm for 30 min. After each filtration, supernatant was diluted to the initial volume with buffer. UV-Vis spectra of each filtrate were recorded and filtration was repeated until negligible MTX signal at λ 371 nm was observed in the last filtrate (5 times). A solution of 75 μM MTX in the absence of the nanoparticles was filtered 5 times in the same way in order to estimate the retention provided by the filter itself, if any.

RESULTS AND DISCUSSION

Synthesis of AuNPs 1-3. The synthesis of AuNPs **1-3** (Scheme 1) was achieved by the well-known ligand exchange strategy on cAuNPs.[57] To this aim, bisalkyltetra(ethylene glycol) disulfides **9** and **10** appended with β-D-lactose and β-CD moieties, respectively, were

synthesized in two steps starting from azide **4** (see Supporting Information).[32] Firstly, regiospecific copper(I)-catalysed azide/alkyne cycloaddition (CuAAC) of **4** with propargyl β-D-lactoside **5** and monopropargyl-β-CD **6** afforded, in this order, the thioacetates **7** (83 %) and **8** (77 %) where new 1,2,3-triazole rings were created. The formation of these rings was easily observed in ^{1}H NMR by the appearance of a singlet at around δ 8.05 ppm. Similarly, two characteristic peaks at around δ 144 and 125 ppm were noticed on the ^{13}C NMR spectra for both products. In addition, IR showed the disappearance of the band at 2101 cm^{-1} initially observed in the spectrum of compound **4** due to the consumption of the free azide group during the CuAAC. Thioacetates **7** and **8** where then deacetylated with an aqueous solution of KOH, which subsequently provoked the oxidation of the resulting thiols into disulfides **9** and **10** in 54 and 69 %, respectively. As expected, disulfides **9** and **10** turned out to be freely soluble in water. Deacetylation of **7** and **8** was easily confirmed in ^{13}C NMR by the disappearance of the peaks corresponding to the carbonyl groups at around δ 196.0 ppm, as well as those assigned to the CH_3 groups at 30.6 ppm. In addition, disulfide formation led to a diamagnetic shift of *ca.* 0.15 ppm for the triplet assigned in ^{1}H NMR to the protons of the methylene directly bound to the sulfur atom. In contrast, the ^{13}C signal for the corresponding carbon showed a shift of *ca.* 8 ppm to lower field.

With disulfides **9** and **10** in hand, we performed ligand exchange reactions on previously prepared citrate-capped nanoparticles (cAuNP). The average diameter of the gold core for cAuNP was determined by transmission electron microscopy (TEM) as 12.1 ± 1.0 nm. However, dynamic light scattering (DLS) showed a hydrodynamic diameter slightly larger (15.2 ± 4.2 nm), which is consistent with the presence of citrate molecules anchored on the surface.[9,31] A mixture of cAuNP and excesses of ligands **9** or **10** in MilliQ water yielded, after 16 hours, AuNPs **1** and

2 appended with β-D-lactose and β-CD moieties, respectively. Similarly, cAuNP was treated in the same conditions with a 1:1 mixture of **9** and **10** to obtain AuNP **3** bearing simultaneously disaccharide and macrocycle moieties. Resulting glycoAuNPs were purified by repetitive centrifugal filtration, washing with pure water in order to remove the excess of ligands.

The exchange process was confirmed firstly by UV-Vis spectroscopy, where a bathochromic shift of 6 nm in the surface plasmon resonance (SPR) band was observed in all cases probably due to the change in the dielectric environment of the metal surface upon the self-assembled monolayer (SAM) formation (Figure 1).[57] In addition, hydrodynamic diameters for AuNPs **1**, **2** and **3** measured by DLS increased from 15.2 ± 4.2 nm for cAuNP to 19.6 ± 4.5 nm, 21.3 ± 4.0 nm and 20.6 ± 3.7 nm, respectively, due to the presence of larger molecules than citrate on the nanoparticle surface after the exchange reaction. In contrast, TEM images showed that the diameter of the gold core remained unchanged, indicating that the functionalization of the cAuNPs with the ligands did not affect to the metallic structure of nanoparticle (Figure 1). The nature of the ligands deposited on the nanoparticles surface was confirmed by ^{1}H NMR spectroscopy. As expected, spectra of the glyconanoparticles matched those previously measured for free **9** and **10** (Supporting Information). In the case of the hybrid AuNP **3**, integral values suggested that linkers containing lactose would be three-times more concentrated on the nanoparticle than those appended with CD moieties. However, this must be considered as estimation since packing density and dissimilar sizes may affect to the spin-spin relaxation time (T2) of each linker in a different extension.[2] Prepared glycoAuNPs showed to be stable in solution since neither aggregation nor SPR band change were observed over a period of several months when stored at 4 ºC in the dark.

Interaction of AuNPs 1 and 3 with lectins PNA and Gal-3. The binding ability of AuNPs **1** and **3** toward β-D-galactose-specific lectins peanut agglutinin (PNA) and human galectin-3 (Gal-3) was tested by following their UV-Vis spectra variation upon the addition of these proteins. This technique has previously been used to demonstrate protein-induced aggregation of AuNPs[27,32-42] due to the well-known dependence of the SPR band on the inter-particle distance.[3] When AuNPs are joined together into an aggregate and distances between them are small enough, their surface plasmons couple changing the local refractive index around the nanoparticles and the SPR band undergoes a red shift and usually a significant broadening which in occasions results in absorbance decay. These phenomena depend on the specific spatial arrangement of the particles after the aggregation and the size of the aggregate. Thus, factors such as AuNP and protein sizes, linker lengths and ligand densities affect to the UV-Vis response of each AuNP-protein pair.

Therefore, 2 nM lactose-containing AuNPs **1** and **3** solutions were firstly treated with 2 μM PNA (Figure 2). This protein is a well-known tetrameric lectin which possesses four β-D-galactose binding sites and thus it is expected to interact with **1** and **3** in a multivalent fashion. Experiments were carried out in 10 mM phosphate buffer at pH 7.2 containing 20 mM NaCl in order to keep a high ionic strength to ensure the stability of the protein and avoid its aggregation. Initially, a progressive increase of the SPR band absorbance (A_{SPR}) with time was observed in both cases. After 60 minutes, however, A_{SPR} started to decay and a dark-red precipitate appeared at the bottom of the cuvette. This decrease was more remarkable in the case of AuNP **3**, the A_{SPR} of which after 3 hours was even less than that observed in the absence of PNA. These results can be reasoned in terms of the formation of cross-linked complexes that increased in size with time. At initial stages of the aggregation the growth of the complexes would increase light scattering in

the sample, causing the observed rise in the absorbance. Nevertheless, after a certain period of time aggregates would reach a critical size which would make them no longer water soluble, leading to their precipitation and the concomitant absorbance decrease. Somewhat surprisingly, AuNP **3** exhibited much more intense precipitation than AuNP **1**. This result would indicate that larger cross-linked complexes are achieved by AuNP **3** although it presents less lactose moieties on its surface than AuNP **1**. It has been shown that high ligand densities on AuNPs are not always optimal as it depends on the target protein dimensions and other structural aspects as the linker length.[27] Furthermore, CD moieties on AuNP **3** might contribute to this behavior, as it is known that the presence of carbohydrates other than those interacting with the lectin can result in a binding enhance.[58] In contrast, the inflexion time for the absorbance variation is around 2 hours for both AuNPs **1** and **3**, suggesting that binding kinetics of these two nanoparticles to PNA seem to be similar despite of the different lactose content.

Addition of PNA to solutions of AuNPs **1** and **3** also had an effect on the SPR band wave-length (λ_{SPR}). In the case of hybrid AuNP **3**, λ_{SPR} underwent a red-shift from 524 nm to 526 nm after 30 minutes. This can be ascribed to the nanoparticles closer spatial arrangement achieved in the cross-linked binding aggregate. However, AuNP **1** showed a more complex behavior since λ_{SPR} depicted an initial shift to shorter wave-lengths from 524 nm to 520 nm in 30 minutes before moving back to 523 nm after 2 hours. This result suggests that AuNP **1** may present some degree of aggregation in the absence of PNA. In our case, observed λ_{SPR} shifts are rather small as compared to those reported for lectins other than PNA in literature.[27,32-42] To the best of our knowledge, studies involving the interaction of gold glyconanoparticles toward PNA lectin in solution are very limited. Wang et al. described λ_{SPR} shifts of ~ 45-55 nm when using AuNPs functionalized with D-galactose and α-1,3-galactobiose.[42] However, those AuNPs were larger (~

20 nm) while linkers were shorter than ours, and therefore inter-particle distances shorter than the core diameter were easier to achieve.

Precipitates obtained from AuNPs **1** and **3** after 5 hours in the presence of PNA were easily re-dissolved in 1 minute upon addition of solid D-lactose to the cuvettes until a final concentration of 40 mM, which also made the SPR band move back to the original λ_{SPR} at 524 nm (Figure 2). These observations showed not only that the PNA-AuNP interaction is reversible but also that such interaction occurs by means of biospecific molecular recognition of the lactose moieties present on AuNP **1** and **3**.

Next, we studied the interaction of AuNP **1** and **3** with Gal-3. To the best of our knowledge, this is the first study on the interaction of gold glyconanoparticles with Gal-3 lectin in solution. Unlike PNA, Gal-3 is a monomeric lectin under the experiment conditions[22] and hence, it is not expected to form a cross-linked complex upon binding interaction with AuNP **1** and **3**. Therefore, changes on their UV-Vis spectra upon interaction with this protein would only derive from the variation of the dielectric constant around the gold core, and in consequence are expected to be much more subtle than those caused by PNA. In fact, the effect of the addition of 2 μM Gal-3 to 2 nM AuNP **1** was negligible (see Supporting Information). In order to obtain a clear UV-Vis response, a concentration of 50 μM for Gal-3 was used. As can be seen from Figure 3, addition of such amount to AuNP **1** and **3** initially caused the absorbance of the SPR band to rise, faster in the case of the latter. After 10 min, A_{SPR} for AuNP **3** began to decrease, reaching the lower limit in 1.5 h. However, this did not happen in the case of the AuNP **1**. SPR bands underwent very little blue shifts (< 2 nm) in both cases. In order to ensure these changes were not due to non-specific interactions, we performed additional control experiments with bovine serum albumin (BSA) under the same conditions which showed negligible effects on

AuNPs SPR bands after 5 hours indicating that non-specific contributions were insignificant (see Supporting Information). These data suggest that increase of A_{SPR} upon addition of Gal-3 would obey to the binding of the lectin to the lactose moieties attached on the nanoparticles. The participation of the carbohydrate in the binding was tested through the addition of solid lactose to the incubating samples after a period of incubation of 5 h. In the case of AuNP **1**, this action resulted in a clear decrease in A_{SPR} as well as a red-shift of 1 nm in λ_{SPR} after 5 min. Behavior of AuNP **3** was, however, more complex as A_{SPR} initially increased due to the formation of a suspension of a non-identified solid in the cuvette. This solid settled with time, leading to lower A_{SPR}. Since it is known that Gal-3 can aggregate when bound to surface ligands,[59] this result might suggest that a fraction of the protein aggregated during its binding to AuNP **3**. The addition of lactose would then cause not only the depletion of the lectin from the nanoparticle but also its incorporation to cross-linked complexes.

Loading of methotrexate (MTX) by AuNPs 2 and 3. In order to evaluate the loading abilities of cyclodextrin-containing AuNPs **2** and **3** toward anti-cancer drugs, we chose MTX (Chart 1) as model since this folic acid analogue is a well-known guest for β-CD and its derivatives.[12-14] Therefore, AuNP **2** and **3** (2 nM) were shaken at room temperature in the presence of an excess of MTX (75 μM). After 5 days in the darkness, repetitive centrifugal filtrations were performed to remove the unbound drug (see Experimental for further details). We recorded the UV-Vis spectra of the subsequent filtrates in order to estimate the presence of MTX by following the variation of the band at λ 371 nm. After 5 filtrations, the amount of MTX found in the corresponding filtrate was negligible. The UV-Vis spectrum of the resulting supernatant was then compared with that for the original mixture after 5 days of incubation. As can be seen from Figure 4, MTX band decreased in all cases but did not disappear, suggesting

that a fraction of the drug added was retained in the supernatant. Furthermore, a 2 nm red-shift was observed in the SPR band of AuNPs **2** and **3**, both of them depicting CD moieties on their structures. In order to discard a holding effect due to the filter, the same experiment was repeated in the absence of any AuNP. In that case, no MTX was found in the supernatant after 5 washes (see Supporting Information). This result indicates that the filter is not able to retain MTX by itself, and thus the drug retention in the supernatant is likely due to its complexation with the AuNPs. Decrease percentages were estimated taking the absorbance at λ 371 nm of each AuNP in the absence of MTX as reference. MTX absorbance decrease was around 70 % when AuNP **1** containing only lactose residues was tested. In sharp contrast, AuNP **2** and **3** led to A_{371} drops of 36 and 32 %, respectively. Taking into account the quenching effect that might operate on the drug upon complexation,[60] these data should be considered as apparent. The higher the decrease percentage is, the lesser the amount of retained MTX is. Thus, these results suggest that MTX retention is clearly higher in the case of AuNP that contain linkers decorated with β-CD moieties, which would indicate that in the case of this drug complexation is mainly due to the drug encapsulation in the cavities of these macrocycles rather than within the linkers themselves.

Conclusions. In summary, we have described the preparation of three gold nanoparticles containing multiple copies of lactose, β-CD and both simultaneously. The potential ability of such nanoparticles as targeted drug delivery systems for anticancer drugs was evaluated by studying their affinities for the β-D-galactose-recognizing lectins PNA and Gal-3 as biological targets. Both proteins demonstrated to interact with the lactose-containing nanoparticles as they induced evident changes in the optical properties of the latter. In contrast, BSA protein did not modify the UV-Vis spectra of these compounds under the same conditions. We also estimated the loading capability of these glyconanoparticles toward the folic acid analogue methotrexate

(MTX). UV-Vis experiments indicated that the presence of CD moieties on the nanoparticles clearly enhanced their abilities to load this anticancer drug. Both features make our hybrid AuNP a potential site-specific delivery system for anticancer drugs.

ACKNOWLEDGMENTS

The authors acknowledge the Andalusian Government (Consejería de Economía, Innovación y Ciencia, grant FQM6903), the Spanish Ministry of Economy and Competitiveness-ERD Fund (grant CTQ2010-17848), and Marie Curie ITN program (CYCLON 237962) for financial support.

Supporting Information Available: Synthesis, characterization data, and ^{1}H NMR, ^{13}C NMR and MALDI-TOF spectra for compounds **1-3** and **7-10**. UV-Vis spectra for the interaction of 2 nM AuNP **1** with 2 μM Gal-3, for AuNPs **1** and **3** in the presence of 50 μM BSA, and for 75 μM MTX before and after five centrifugal filtrations. This material is available free of charge via the Internet at http://pubs.acs.org.

REFERENCES

1. The term “gold nanoparticle” usually referrers gold nanospheres (although they are not strictly spheres but a collection of polyhedral such as decahedra, dodecahedra, icosahedra and, predominantly, truncated cuboctahedra) and so it will be used in this paper. More recently new shapes have been developed such as nanorods, nanostars, nanocubes and nanoshells. See: Thakor, A. S., Jokerst, J., Zaveleta, C., Massoud, T. F., and Gambhir, S. S. (2011) Gold nanoparticles: a revival in precious metal administration to patients. *Nano Lett. 11*, 4029-4036.

2. Daniel, M.-C., and Astruc, D. (2004) Gold nanoparticles: assembly, supramolecular chemistry, quantum-size-related properties, and applications toward biology, catalysis, and nanotechnology. *Chem. Rev. 104*, 293-346.

3. Marradi, M., Martín-Lomas, M., and Penadés, S. (2010) Glyconanoparticles: polyvalent tools to study carbohydrate-based interactions. *Adv. Carbohydr. Chem. Biochem. 64*, 211-290.

4. Jans, H., and Huo, Q. (2012) Gold nanoparticle-enabled biological and chemical detection and analysis. *Chem. Soc. Rev. 41*, 2849-2866.

5. Saha, K., Agasti, S. S., Kim, C., Li, X., and Rotello, V. M. (2012) Gold nanoparticles in chemical and biological sensing. *Chem. Rev. 112*, 2739-2779.

6. Vilela, D., González, M. C., and Escarpa, A. (2012) Sensing colorimetric approaches based on gold and silver nanoparticles aggregation: chemical creativity behind the assay. A review. *Anal. Chim. Acta 751*, 24-43.

7. Rana, S., Bajaj, A., Mout, R., and Rotello, V. M. (2012) Monolayer coated gold nanoparticles for delivery applications. *Adv. Drug Deliv. Rev. 64*, 200-216.

8. Gimenez, I. F., Anazetti, M. C., Melo, P. S., Haun, M., De Azevedo, M. M. M., Durán, N., and Alves, O. L. (2005) Cytotoxicity on V79 and HL60 cell lines by thiolated-β-cyclodextrin-Au/violacein nanoparticles. *J. Biomed. Nanotech. 1*, 352-358.

9. Park, C., Youn, H., Kim, H., Noh, T., Kook, Y. H., Oh, E. T., Park, H. J., and Kim, C. (2009) Cyclodextrin-covered gold nanoparticles for targeted delivery of an anti-cancer drug. *J. Mater. Chem. 19*, 2310-2315.

10. Jeong, S.-Y., Park, S.-J., Yoon, S. M., Jung, J., Woo, H. N., Yi, S. L., Song, S. Y., Park, H. J., Kim, C., Lee, J. S., Lee, J. S., and Choi, E. K. (2009) Systemic delivery and preclinical evaluation of Au nanoparticle containing β-lapachone for radiosensitization. *J. Control. Release 139*, 239-245.

11. Heo, D. N., Yang, D. H., Moon, H.-J., Lee, J. B., Bae, M. S., Lee, S. C., Lee, W. J., Sun, I.-C., and Kwon, I. K. (2012) Gold nanoparticles surface-functionalized with paclitaxel drug and biotin receptor as theranostic agents for cancer therapy. *Biomaterials 33*, 856-866.

12. Pattarino, F., Giovannelli, L., Giovenzana, G. B., Rinaldi, M., and Trotta, M. (2005) Inclusion of methotrexate in alkyl-cyclodextrins: effects of host substituents on the stability of complexes. *J. Drug. Deliv. Sci. Tech. 15*, 465-468.

13. Deng, J., Li, N., Mai, K., Yang, C., Yan, L., and Zhang, L.-M. (2011) Star-shaped polymers consisting of a β-cyclodextrin core and poly(amidoamine) dendron arms:

binding and release studies with methotrexate and siRNA. *J. Mater. Chem. 21*, 5273-5281.

14. Aykaç, A., Martos-Maldonado, M. C., Casas-Solvas, J. M., García-Fuentes, L., and Vargas-Berenguel, A. (2012) Binding ability properties of β-cyclodextrin dimers linked through their secondary faces towards cancer chemotherapeutic agent methotrexate. *J. Drug Deliv. Sci. Tech. 22*, 270-272.

15. Oda, Y., Kobayashi, N., Yamanoi, T., Katsuraya, K., Takahashi, K., and Hattori, K. (2008) β-Cyclodextrin conjugates with glucose moieties designed as drug carriers: their syntheses, evaluations using concanavalin A and doxorubicin, and structural analyses by NMR spectroscopy. *Med. Chem. 4*, 244-255.

16. Thiele, C., Auerbach, D., Jung, G., and Wenz, G. (2011) Inclusion of chemotherapeutic agents in substituted β-cyclodextrin derivatives. *J. Incl. Phenom. Macrocycl. Chem. 69*, 303-307.

17. Yunomae, K., Arima, H., Hirayama, F., and Uekama, K. (2003) Involvement of cholesterol in the inhibitory effect of dimethyl-β-cyclodextrin on P-glycoprotein and MRP2 function in Caco-2 cells. *FEBS Lett. 536*, 225-231.

18. Fenyvesi, F., Fenyvesi, E., Szentc, L., Goda, K., Bacsó, Z., Bácskay, I., Váradi, J., Kiss, T., Molnár, E., Janáky, T., Szabó, G., Jr., and Vecsernyés, M. (2008) P-glycoprotein inhibition by membrane cholesterol modulation. *Eur. J. Pharm. Sci*. *34*, 236-242.

19. Baek, J.-S., and Cho, C.-W. (2013) 2-Hydroxypropyl-β-cyclodextrin-modified SLN of paclitaxel for overcoming P-glycoprotein function in multidrug-resistant breast cancer cells. *J. Pharm. Pharmacol. 65*, 72-78.

20. Doane, T. L., and Burda, C. (2012) The unique role of nanoparticles in nanomedicine: imaging, drug delivery and therapy. *Chem. Soc. Rev. 41*, 2885-2911.

21. Arvizo, R. R., Bhattacharyya, S., Kudgus, R. A., Giri, K., Bhattacharya, R., and Mukherjee, P. (2012) Intrinsic therapeutic applications of noble metal nanoparticles: past, present and future. *Chem. Soc. Rev. 41*, 2943-2970.

22. Téllez-Sanz, R., García-Fuentes, L., and Vargas-Berenguel, A. (2013) Human Galectin-3 selective and high affinity inhibitors. Present state and future perspectives. *Curr. Med. Chem. 20*, 2979-2990.

23. Vargas-Berenguel, A., Ortega-Caballero, F., and Casas-Solvas, J. M. (2007) Supramolecular chemistry of carbohydrate clusters with cores having guest binding abilities. *Mini-Rev. Org. Chem. 4*, 1-14.

24. Martínez, M., Ortiz-Mellet, C., and García-Fernández J. M. (2013) Cyclodextrin-based multivalent glycodisplays: covalent and supramolecular conjugates to assess carbohydrate–protein interactions. *Chem. Soc. Rev. 42*, 4746-4773.

25. Takae, S., Akiyama, Y., Otsuka. , H., Nakamura, T., Nagasaki, Y., and Kataoka, K. (2005) Ligand density effect on biorecognition by PEGylated gold nanoparticles: regulated interaction of RCA_{120} lectin with lactose installed to the distal end of tethered PEG strands on gold surface. *Biomacromolecules 6*, 818-824.

26. Bergen, J. M., von Recum, H. A., Goodman, T. T., Massey, A. P., and Pun, S. H. (2006) Gold nanoparticles as a versatile platform for optimizing physicochemical parameters for targeted drug delivery. *Macromol. Biosci. 6*, 506-516.

27. Schofield, C. L., Mukhopadhyay, B., Hardy, S. M., McDonnell, M. B., Field, R. A., and Russell, D. A. (2008) Colorimetric detection of *Ricinus communis* Agglutinin 120 using optimally presented carbohydrate-stabilised gold nanoparticles. *Analyst 133*, 626-634.

28. Pale-Grosdemange, C., Simon, E. S., Prime, K. L., and Whitesides, G. M. (1991) Formation of self-assembled monolayers by chemisorption of derivatives of oligo(ethylene glycol) of structure $HS(CH_2)_{11}(OCH_2CH_2)_mOH$ on gold. *J. Am. Chem. Soc. 113*, 12-20.

29. Kanaras, A. G., Kamounah, F. S., Schaumburg, K., Kiely, C. J., and Brust, M. (2002) Thioalkylated tetraethylene glycol: a new ligand for water soluble monolayer protected gold clusters. *Chem. Commun.* 2294-2295.

30. Zhang, F., Skoda, M. W. A., Jacobs, r. M. J., Zorn, S., Martin, R. A., Martin, C. M., Clark, G. F., Goerighk, G., and Schreiber, F. (2007) Gold nanoparticles decorated with oligo(ethylene glycol) thiols: protein resistance and colloidal stability. *J. Phys. Chem. A 111*, 12229-12237.

31. Larson, T. A., Joshi, P. P., and Sokolov, K. (2012) Preventing protein adsorption and macrophage uptake of gold nanoparticles *via* a hydrophobic shield. *ACS Nano 6*, 9182-9190.

32. Martos-Maldonado, M. C., Thygesen, M. B., Jensen, K. J., and Vargas-Berenguel, A. (2013) Gold–ferrocene glyco-nanoparticles for high-sensitivity electrochemical detection of carbohydrate–lectin interactions. *Eur. J. Org. Chem.* 2793-2801.

33. Thygesen, M. B., Sauer, J., and Jensen, K. J. (2009) Chemoselective capture of glycans for analysis on gold nanoparticles: carbohydrate oxime tautomers provide functional recognition by proteins. *Chem. Eur. J. 15*, 1649-1660.

34. Sánchez-Pomales, G., Morris, T. A., Falabella, J. B., Tarlov, M. J., and Zangmeister, R. A. (2012) A lectin-based gold nanoparticle assay for probing glycosylation of glycoproteins. *Biotechnol. Bioeng. 109*, 2240-2249.

35. Otsuka, H., Akiyama, Y., Nagaski, Y., and Kataoka, K. (2001) Quantitative and reversible lectin-induced association of gold nanoparticles modified with α-lactosyl-ω-mercapto-poly(ethylene glycol). *J. Am. Chem. Soc. 123*, 8226-8230.

36. Hone, D. H., Hames, A. H., and Russell, D. A. (2003) Rapid, quantitative colorimetric detection of a lectin using mannose-stabilized gold nanoparticles. *Langmuir 19*, 7141-7144.

37. Lee, S., and Pérez-Luna, V. H. (2005) Dextran−gold nanoparticle hybrid material for biomolecule immobilization and detection. *Anal. Chem. 77*, 7204-7211.

38. Aslan, K., Luhrs, C. C., and Pérez-Luna, V. H. (2004) Controlled and reversible aggregation of biotinylated gold nanoparticles with streptavidin. *J. Phys. Chem. B 108*, 15631-15639.

39. Thygesen, M. B., Sørensen, K. K., Cló, E., and Jensen, K. J. (2009) Direct chemoselective synthesis of glyconanoparticles from unprotected reducing glycans and glycopeptide aldehydes. *Chem. Commun.*, 6367-6369.

40. Deng, Z., Li, S., Jiang, X., and Narain, R. (2009) Well-defined galactose-containing multi-functional copolymers and glyconanoparticles for biomolecular recognition processes. *Macromolecules 42*, 6393-6405.

41. Schofield, C. L., Haines, A. H., Field, R. A., and Russell, D. A. (2006) Silver and gold glyconanoparticles for colorimetric bioassays. *Langmuir 22*, 6707-6711.

42. Wang, X., Ramström, O., Yan, M. (2009) A photochemically initiated chemistry for coupling underivatized carbohydrates to gold nanoparticles. *J. Mater. Chem. 19*, 8944-8949.

43. Mahon, E., Aastrup, T., and Barboiu, M. (2010) Multivalent recognition of lectins by glyconanoparticle systems. *Chem. Commun. 46*, 5491-5493.

44. Jiang, X., Housni, A., Gody, G., Boullanger, P., Charreyre, M.-T., Delair, T., and Narain, R. (2010) Synthesis of biotinylated α-D-mannoside or *N*-acetyl β-D-glucosaminoside decorated gold nanoparticles: study of their biomolecular recognition with Con A and WGA lectins. *Bioconjugate Chem. 21*, 521-530.

45. Wang, X., Ramström, O., and Yan, M. (2011) Dynamic light scattering as an efficient tool to study glyconanoparticle-lectin interactions. *Analyst 136*, 4174-4178.

46. Wang, X., Matei, E., Gronneborn, A. M., Ramström, O., and Yan, M. (2012) Direct measurement of glyconanopaticles and lectin interactions by isothermal titration calorimety. *Anal. Chem. 84*, 4248-4252.

47. Wang, X., Ramström, O., and Yan, M. (2010) Quantitative analysis of multivalent ligand presentation on gold glycnonanoparticles and the impact on lectin binding. *Anal. Chem. 82*, 9082-9089.

48. Hasegawa, T., Umeda, M., Numata, M., Li, C., Bae, A.-H., Fujisawa, T., Haraguchi, S., Sakurai, K., and Shinkai, S. (2006) 'Click chemistry' on polysaccharides: a convenient, general, and monitorable approach to develop (1→3)-β-D-glucans with various functional appendages. *Carbohydr. Res. 341*, 35-40.

49. Casas-Solvas, J. M., Ortiz-Salmerón, E., Fernández, I., García-Fuentes, L., Santoyo-González, F., and Vargas-Berenguel, A. (2009) Ferrocene–β-cyclodextrin conjugates: synthesis, supramolecular behavior, and use as electrochemical sensors. *Chem. Eur. J. 15*, 8146-8162.

50. Perrin, D. D., and Armarego, W. F. L. (1989) *Purification of Laboratory Chemicals, 3rd ed.*, Pergamon, Oxford.

51. Lévi, R., Thank, N. T. K., Doty, R. C., Hussain, I., Nichols, R. J., Schirffrin, D. J., Brust, M., and Ferning, D. G. (2004) Rational and combinatorial design of peptide capping ligands for gold nanoparticles. *J. Am. Chem. Soc. 126*, 10076-10084.

52. Turkevich, J., Stevenson, P. C., and Hillier, J. (1953) The formation of colloidal gold. *J. Phys. Chem. 57*, 670-673.

53. Haiss, W., Thank, N. T. K., Aveyard, J., and Ferning, D. G. (2007) Determination of size and concentration of gold nanoparticles from UV−Vis spectra. *Anal. Chem. 79*, 4215-4221.

54. Hadari, Y. R., Paz, K., Dekel, R., Mestrovic, T., Accili, D., and Zick, Y. (1995) Galectin-8: a new rat lectin, related to Galectin-4. *J. Biol. Chem. 270*, 3447-3453.

55. Porath, J., and Ersson, B. (1973) Biospecific methods for purification and characterization of pneumococcal polysaccharide PnS XIV. *Proceedings of the Symposium on New Approaches for Inducing Natural Immunity to Pyogenic Organisms* (Robbins, J. B., Horton, R. E., Drause, R. M., Eds.), pp 101-108, Winter Park, Florida.

56. Bradford, M. M. (1976) A rapid and sensitive method for the quantitation of microgram quantities of protein utilizing the principle of protein-dye binding. *Anal. Biochem. 72*, 248-254.

57. Weisbecker, C. S., Merritt, M. V., and Whitesides, G. M. (1996) Molecular self-assembly of aliphatic thiols on gold colloids. *Langmuir 12*, 3763-3772.

58. Gómez-García, M., Benito, J. M., Rodríguez-Lucena, D., Yu, J.-X., Chmurski, K., Ortíz-Mellet, C., Gutiérrez-Gallego, R., Maestre, A., Defaye, J., and García-Fernández, J. M. (2005) Probing secondary carbohydrate−protein interactions with highly dense cyclodextrin-centered heteroglycoclusters: The heterocluster effect. *J. Am. Chem. Soc. 127*, 7970-7971.

59. Vrasidas, I., André, S., Valentini, P., Böck, C., Lensch, M., Kalter, H., Liskamp, R. M. J., Gabius, H.-J., and Pieters, R. J. (2003) Rigidified multivalent lactose molecules and their

interactions with mammalian galectins: a route to selective inhibitors. *Org. Biomol. Chem. 1*, 803-810.

60. François, A., Laroche, A., Pinaud, N., Salmon, L., Ruiz, J., Robert, J., and Astruc, D. (2011) Encapsulation of docetaxel into PEGylated gold nanoparticles for vectorization to cancer cells. *ChemMedChem 6*, 2003-2008.

SCHEMES AND CHARTS

Chart 1. Anticancer drug methotrexate (MTX)

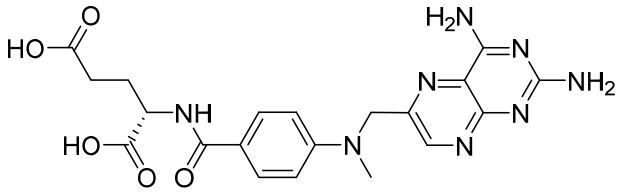

Scheme 1. Synthesis of AuNPs **1-3**

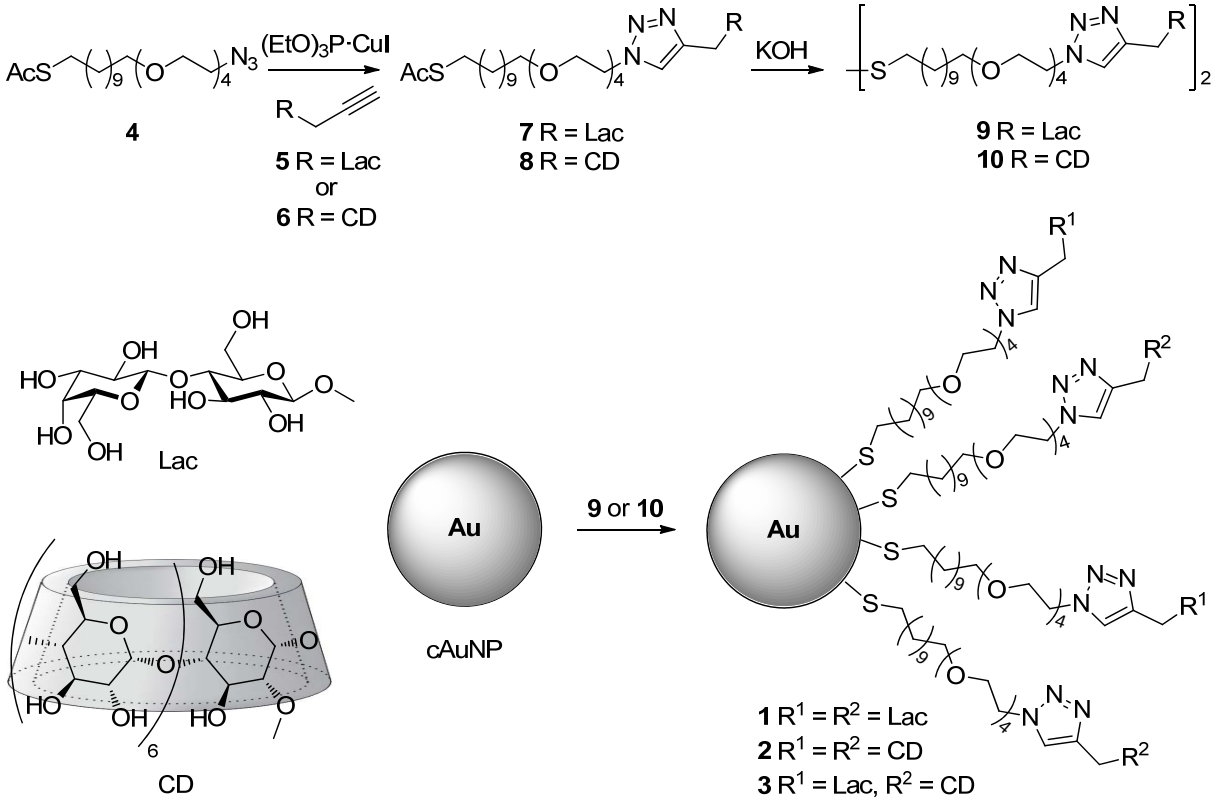

FIGURES

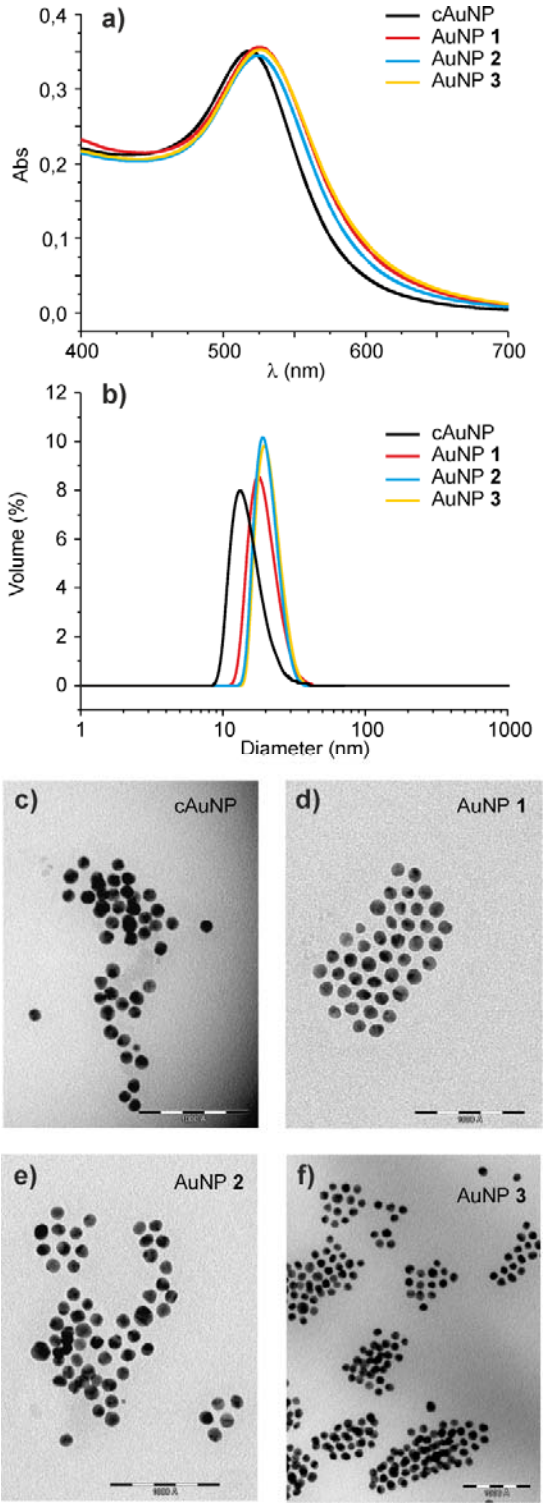

Figure 1. (a) UV-Vis spectra for cAuNP and AuNPs **1-3**. (b) DLS size distribution of cAuNP and AuNPs **1-3** at a scattering angle of 173º. (c-f) TEM images of cAuNP and AuNPs **1-3**.

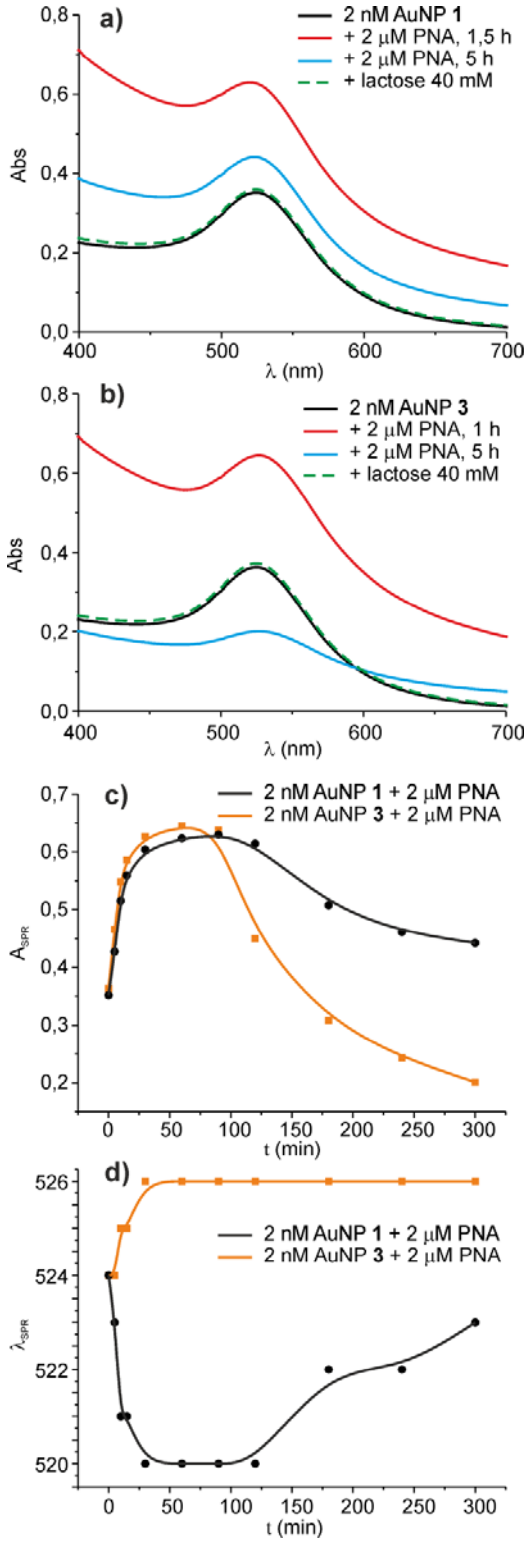

Figure 2. UV-Vis spectra for (a) AuNP **1** (2 nM) and (b) AuNP **3** (2 nM) in 10 mM phosphate buffer, pH 7.2, 20 mM NaCl in the absence and in the presence of 2 μM PNA after incubation at room temperature in the dark. Variation of (c) A_{SPR} and (d) λ_{SPR} with time for 2 nM AuNP **1** and AuNP **3** in the presence of 2 μM PNA in 10 mM phosphate buffer, pH 7.2, 20 mM NaCl.

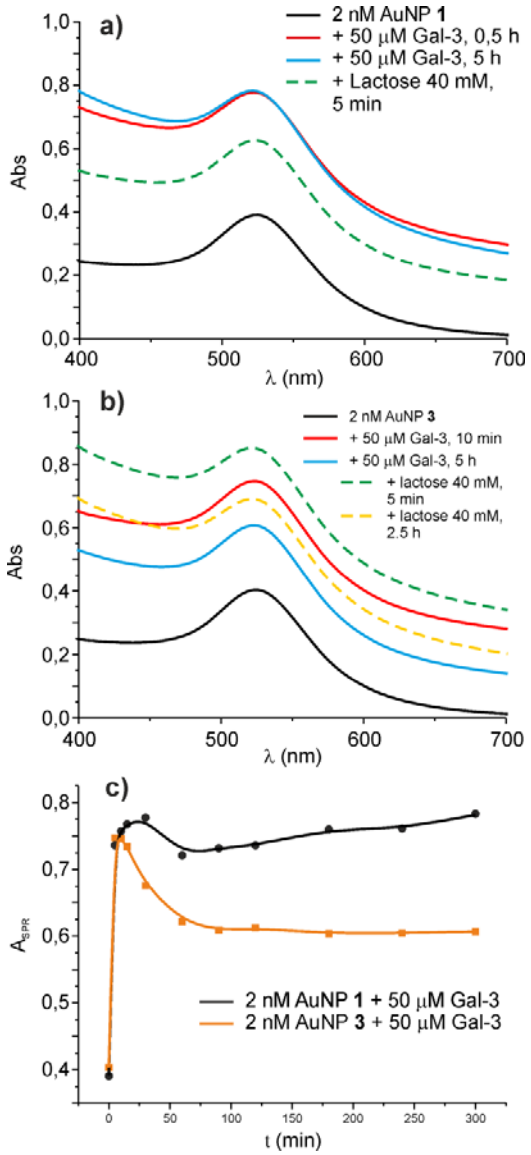

Figure 3. UV-Vis spectra for (a) AuNP **1** (2 nM) and (b) AuNP **3** (2 nM) in 10 mM phosphate buffer, pH 7.2, 20 mM NaCl in the absence and in the presence of 50 µM Gal-3 after incubation at room temperature in the dark. (c) Variation of A_{SPR} with time for 2 nM AuNP **1** and AuNP **3** in the presence of 50 µM Gal-3 in 10 mM phosphate buffer, pH 7.2, 20 mM NaCl.

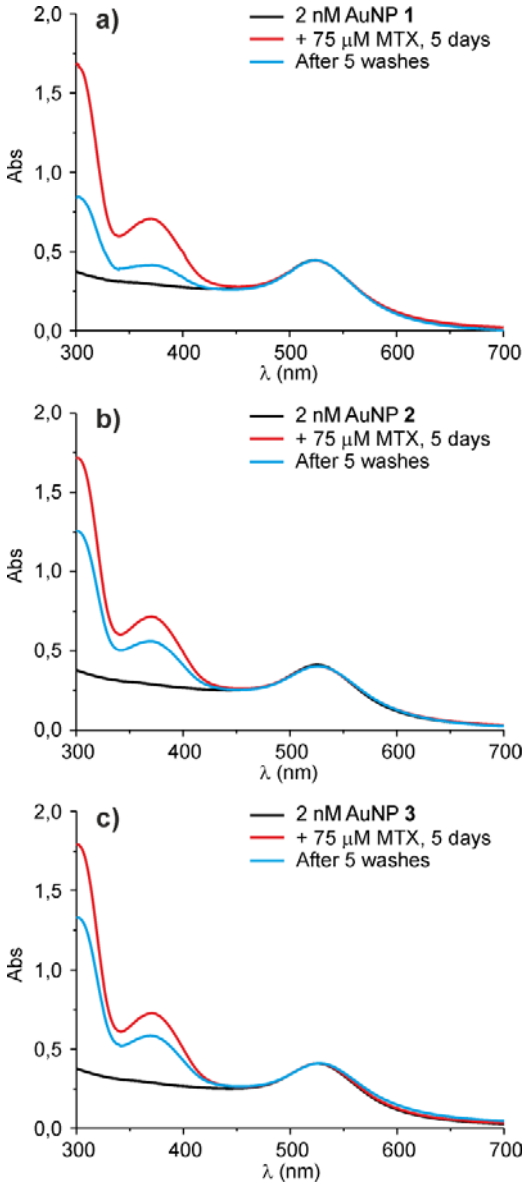

Figure 4. (a-c) UV-Vis spectra for AuNPs **1-3** (2 nM) in 10 mM phosphate buffer, pH 7.2, 20 mM NaCl before and after their incubation in the presence of 75 µM MTX at room temperature in the dark for 5 days. The figure also shows the UV-Vis spectra of the supernatant resulting after 5 washes with buffer in order to remove the excess of unbound drug.

β-Cyclodextrin-bearing Gold Glyconanoparticles for the Development of Site Specific Drug Delivery Systems.

Ahmet Aykaç, Manuel C. Martos-Maldonado, Juan M. Casas-Solvas, Indalecio Quesada-Soriano, Federico García-Maroto, Luís García-Fuentes, and Antonio Vargas-Berenguel

TABLE OF CONTENTS (TOC) GRAPHIC